Hindawi
Journal of Advanced Transportation
Volume 2019, Article ID 9182761, 9 pages
https://doi.org/10.1155/2019/9182761

Research Article

Decoupling Control Strategy of IPT System Based on Optimal Efficiency Load Tracking

Wenmei Hao, Liwei Zhang, Sanmu Xiu, and Fengyu Leng

School of Electrical Engineering, Beijing Jiaotong University, Beijing 100044, China

Correspondence should be addressed to Liwei Zhang; lwzhang@bjtu.edu.cn

Received 8 February 2019; Revised 29 March 2019; Accepted 31 March 2019; Published 11 April 2019

Academic Editor: Luca Pugi

The inductive power transmission system is applied to urban rail transit. Due to the limitations of the volume and coupling coefficient of the inductive coupling mechanism and the fact that the fluctuation of air gap in its movement will cause the fluctuation of mutual inductance value, DCDC booster link should be added to the side, rectifying side, to improve the output voltage level and stability. At present, most of the existing control strategies are based on the original side information communication. However, in the application of dynamic wireless charging in urban rail transit, the primary and secondary side coils are in the process of relative movement, so it is relatively difficult to establish reliable real-time communication, and it is easy to be interfered by electromagnetic transmission process, resulting in large errors. This paper analyzes the relationship between load and efficiency of IPT system applied to urban rail transit in detail and obtains the optimal load matching strategy of optimal efficiency. At the same time, an independent control strategy is proposed to eliminate the information communication of the primary and secondary sides and realize decoupling control. Finally, a simulation model is built to verify the effectiveness of the control strategy.

1. Introduction

With the continuous development of urban transportation, environment-friendly urban rail transit vehicles have become an important part of the strategic framework of urban comprehensive transportation development. However, there are many disadvantages in the power supply mode of overhead contact network, such as friction electric spark, poor landscape, and so on. The inductive power transmission (IPT) technology is to transfer the power from the power supply to the power load in a noncontact way, which has the advantages of safety, reliability, and flexible power supply. Therefore, the high-power induction power transmission technology and its application in urban rail transit have become the focus of research at home and abroad in recent years [1].

The IPT system is applied to urban rail transit. In order to keep the vehicle running stably, its output voltage and power level are strictly limited to a predetermined range. However, the device volume and coupling coefficient of inductively coupled mechanism based on loosely coupled transformer have certain limitations, and its direct output voltage often cannot reach the present range. The variation of mutual inductance due to the fluctuation of air gap and the equivalent load due to the change of power demand will lead to the fluctuation of output voltage and affect the stability of the system. Therefore, it is necessary to add DCDC booster voltage link after diode rectification circuit of traditional IPT system to reduce output requirements of coupling mechanism [2]. At present, most of the existing control strategies are based on the information communication between the primary and secondary sides [3, 4], with few studies on decoupling and independent control. However, in the application of dynamic wireless charging in urban rail transit, the primary and secondary side coils are in the process of relative movement, so it is relatively difficult to establish reliable real-time communication, and it is easy to be interfered by electromagnetic transmission process, resulting in large errors. Therefore, the establishment of an independent control mode to avoid the information transfer between the primary and secondary sides can greatly improve the transmission capacity of the system and improve the timeliness of the system.

Aimed at the dynamic IPT system applied to urban rail transit, this paper proposes a decoupling control strategy of

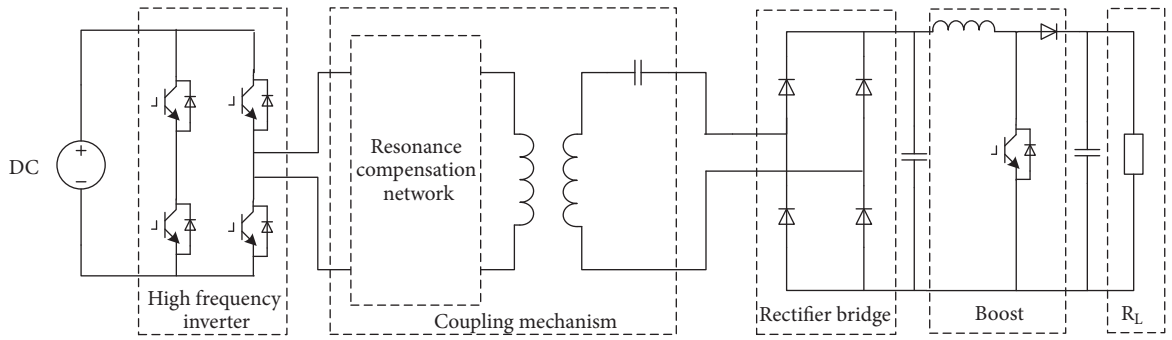

Figure 1: Structure of IPT system applied to urban rail transit.

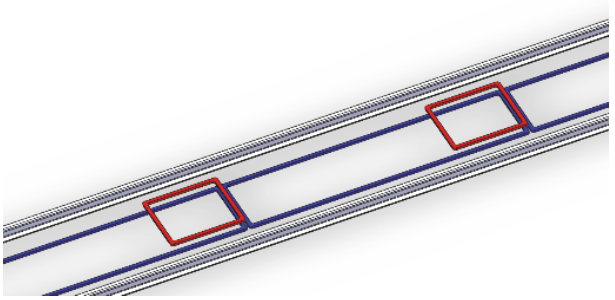

Figure 2: Configuration of primary and secondary coils.

primary and secondary sides based on the optimal efficiency. Firstly, the air gap fluctuation between the system structure and the actual running of the vehicle is analysed. Finite element method is used to simulate the variation law of mutual inductance parameters in the case of air gap fluctuation, and the resonant compensation topology with optimal output capability is selected based on mutual inductance range. In the process of dynamic operation of vehicles, mutual inductance changes caused by air gap fluctuations are inevitable. On this basis, an efficient decoupling control method of the primary and secondary sides is proposed, so that the system can maintain a high efficiency output within the range of mutual inductance parameters. Finally, simulation verifies the effectiveness of the control strategy.

2. Coupling Mechanism Analysis

100% low-floor trams in this paper are the research object; the system structure is shown in Figure 1. The primary side inverts the dc voltage into high-frequency alternating current through a high-frequency inverter and then transfers it to the secondary side through an inductively coupled mechanism. The secondary side rectifies the induced high-frequency current into dc output through noncontrol rectifier and realizes the output of energy by boosting DCDC converter. Since the secondary side is installed on the vehicle, its space position is limited and its resonance frequency should be stable, so the basic series (S-type) resonant compensation topology is selected for the secondary side.

2.1. Mutual Inductance Parameter. According to the dynamic transmission characteristics of the system, the coil configuration mode of the primary side long and the secondary side short as shown in Figure 2 is proposed. On the basis of the installation space of the existing noncatenary tram, it is determined that the primary coil adopts a rectangular coil of 20 m∗1 m and the secondary coil is a square coil of 1 m∗1 m. The coil adopts the basic d-type coil structure, which has the characteristics of small mutual inductance attenuation under transverse deviation, and at the same time increases the smoothness at the folding angle to reduce the magnetic field distortion. In order to improve the mutual inductance of the system and reduce the coil loss as much as possible, the primary side adopts two-circle winding, and the secondary side adopts five-circle winding to meet the output voltage requirement.

The coil configuration with long primary coil can keep the magnetic field in the middle of the coil stable, and the magnetic field fluctuation at the coil boundary decreases with the increase of distance. Therefore, the parameter fluctuation caused by the horizontal motion of the coil is ignored, and only the mutual inductance fluctuation caused by the change of air gap in the vertical direction of the coil is considered. The air gap fluctuation of the vehicle during movement is shown in Table 1.

The variation range of air gap in the table is 37.6mm-127mm. Finite element simulation analysis was carried out on the coupling mechanism under different air gaps in ANSYS Maxwell, and the mutual inductance change curve was obtained as shown in Figure 3. It can be seen from

Table 1: Air gap fluctuation during movement.

	AW0	AW2	AW3
Dynamic variation	55	62,6	64,4
Range of air gap	72-127	44,4-107	37,6-102

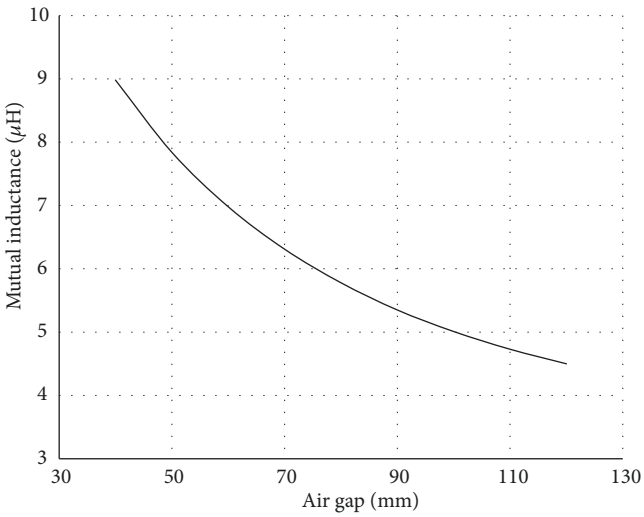

Figure 3: Mutual inductance variation.

the image that, along with the increase of air gap, mutual inductance decreases; mutual inductance fluctuation range is 9μH to 4.5μH. The following studies all aim at the variation range of mutual inductance.

2.2. Topology Selection of Primary Resonant Compensation. In the short action time of urban rail transit dynamic wireless charging, full reliability on the primary side/secondary side of the stability control strategy to achieve high power transmission still faces certain difficulty, so it is necessary in the process of system design to choose the appropriate harmonic compensation topology and keep the system under the range of mutual inductance high power output.

At present, the research on resonant compensation network mainly focuses on the following compensation structures: element compensation, series parallel compensation, and series parallel series compensation of three elements. Basic element compensation topology (S, P) has been studied a lot [3, 4]. Combined with the advantages of s-type and p-type resonances, literatures [5, 6] describe the series parallel type two-element compensation (LCL), which can provide high voltage and current gain without increasing switching stress. The literature [1, 7] proposed series parallel series three-element compensation (LCC), which inherited all the advantages of LCL compensation network and increased the compensation capacitor C_P compared with series parallel LCL compensation circuit, thus adding one degree of freedom in the design process. Based on the analysis in the previous section, the secondary side adopts S-type compensation, and the topology of S, P, LCL, and LCC resonant compensation adopted by the primary side is shown in Figures 4(a), 4(b), 4(c), and 4(d).

In the figures, U_{in} is the RMS value of the voltage base wave output of the inverter, L_r, C_r, and C_p are the resonant compensation elements of the primary side, L_p is the self-inductance of the primary side coil, C_s is the resonant compensation element of the secondary side, L_s is the self-inductance of the secondary side coil, R_{eq} is the equivalent resistance of the output side of the secondary side, and R_p, R_{Lr}, and R_s are the parasitic inductance resistance.

The circuits in Figures 4(a), 4(b), 4(c), and 4(d) are analysed separately and the following assumptions are made [8]:

(1) All inverter circuit components are ideal.

(2) The inverter circuit operates in soft switching mode, so the switching losses of the inverter are assumed to be zero because it works in zero-voltage switching [9].

(3) The working frequency of the system inverter circuit is equal to the resonance angular frequency that is ω, and the primary side inductance L_p and L_s are determined by the coupling mechanism design.

(4) The system operates at a high frequency and the parasitic resistance of inductance is relatively small, but its influence cannot be ignored. However, the product of the two parasitic resistors can be approximately ignored; that is, $R_sR_p = 0$ or $R_sR_{Lr} = 0$ or $R_pR_{Lr} = 0$.

Based on this, four resonant compensation topological parameter relations can be analyzed as shown in Table 2. Z_r is the side reflection impedance and Z_{in} is the equivalent impedance of the input side.

In the range of mutual inductance that can be achieved by the system in the previous section, the variation trend of output power and efficiency of the four topologies with mutual inductance under the same parameter is obtained, as shown in Figures 5(a), 5(b), 5(c), and 5(d).

As can be seen from the image, the output power of the four topologies increases with the mutual inductance. However, compared with the other three compensation topologies, the primary S-type resonant compensation topology has a very strong power output capacity and is suitable for high-power applications. As can be seen from Figures 5(b) and 5(c), due to the large inductance of the primary side coil, P-type and LCL-type greatly limit the power output capacity of the system. LCC-type (Figure 5(d)) can change its power output capacity according to the value of L_r and has a certain degree of freedom, but the gap is still large compared with S-type. In terms of efficiency, the efficiency output of S-type shows a reverse correlation trend, which is more special than the other three topologies, but the efficiency range of the four topologies is roughly consistent [10].

Therefore, it can be concluded that, under the same system parameters, the output capacity of SS resonant topology

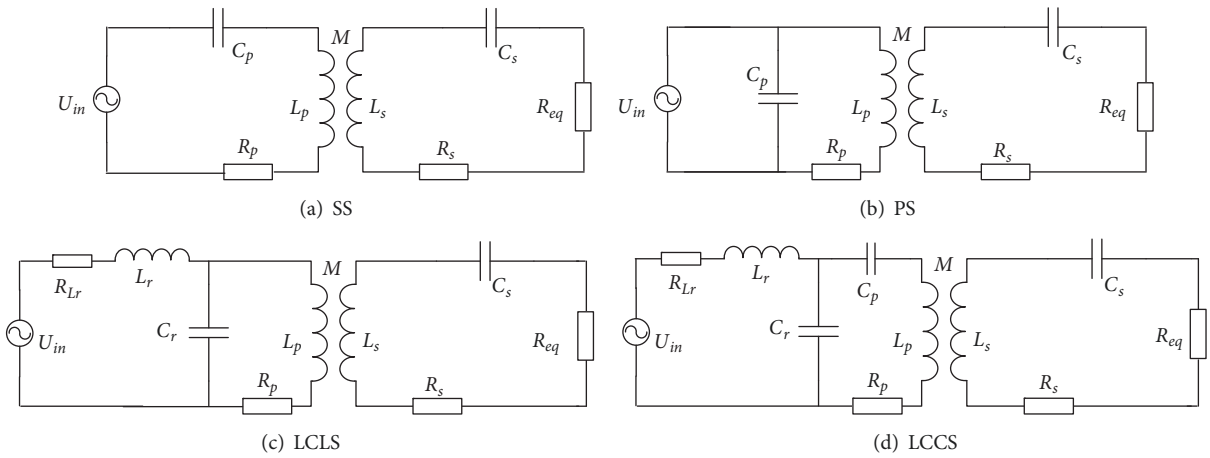

Figure 4: Four resonant compensation topologies.

Table 2: Four topological parameter relationships.

Parameter	SS	PS	LCLS	LCCS
C_s	$\frac{1}{\omega^2 L_s}$	$\frac{1}{\omega^2 L_s}$	$\frac{1}{\omega^2 L_s}$	$\frac{1}{\omega^2 L_s}$
Z_r	$\frac{\omega^2 M^2}{R_s + R_{eq}}$	$\frac{\omega^2 M^2}{R_s + R_{eq}}$	$\frac{\omega^2 M^2}{R_s + R_{eq}}$	$\frac{\omega^2 M^2}{R_s + R_{eq}}$
C_p	$\frac{1}{\omega^2 L_p}$	$\frac{L_p}{\omega^2 {L_p}^2 + \left(\frac{\omega^2 M^2}{R_{eq} + R_s} + R_p\right)^2}$	/	$\frac{1}{\omega^2 \left(L_p - L_r\right)}$
C_r	/	/	$\frac{1}{\omega^2 L_p}$	$\frac{1}{\omega^2 L_r}$
L_r	/	/	L_p	L_r
Z_{in}	$Z_r + R_p$	$\frac{\omega^2 M^2}{Z_r + R_p} + Z_r + R_p$	$\frac{{L_r}^2}{M^2}\left(Z_r + R_p\right)$	$\frac{{L_r}^2}{M^2}\left(Z_r + R_p\right) + R_{Lr}$
P_{out}	$\frac{{U_{in}}^2 \omega^2 M^2 R_{eq}}{\left(R_p R_{eq} + \omega^2 M^2\right)^2}$	$\frac{{U_{in}}^2 \omega^2 M^2 R_{eq}}{\left(R_p R_{eq} + \omega^2 M^2\right)^2 + \left[\omega L_p \left(R_{eq} + R_s\right)\right]^2}$	$\frac{U_{in}^2 \left(\omega^4 M^2 C_r + R_p R_{eq} \omega^2 C_r\right)^2 M^2 R_{eq}}{\left(\omega^2 M^2 + R_p R_{eq}\right)^2 \left[\left(R_{eq} + R_s\right) + R_{Lr} \omega^4 M^2 C_r^2\right]^2}$	
η		$\frac{\omega^2 M^2 R_{eq}}{\omega^2 M^2 \left(R_{eq} + R_s\right) + {R_p}^2 {R_{eq}}^2}$	$\frac{\left(\omega^4 M^2 C_r + R_p R_{eq} \omega^2 C_r\right)^2 M^2 R_{eq}}{\left(\omega^2 M^2 + R_p R_{eq}\right)^2 \left[\left(R_{eq} + R_s\right) + R_{Lr} \omega^4 M^2 C_r^2\right] C_r}$	

is obviously better than the other three, so SS resonant network is selected as the system compensation topology. The following will focus on the efficiency improvement strategy of the system.

3. Optimal Efficiency Tracking Control Strategy

According to the analysis in the previous section, the system has a high output capacity under SS resonant topology, which is suitable for the application of high-power urban rail transit. However, as can be seen from Figure 5(a), the output power of the system decreases with the increase of mutual inductance in the corresponding mutual inductance range, and the efficiency is lower with higher output power. Therefore, this section will analyze the optimal efficiency tracking strategy based on load matching.

From the formula in Table 2,

$$\eta = \frac{\omega^2 M^2 R_{eq}}{\omega^2 M^2 \left(R_{eq} + R_s\right) + {R_p}^2 {R_{eq}}^2} \tag{1}$$

It can be seen that the system efficiency is related to the factors in the formula. When the system hardware is determined, the impedances R_s and R_p of the primary and secondary side coils have been determined [11]. The three-dimensional diagram of the efficiency changing with mutual inductance M and equivalent resistance R_{eq} is shown in Figure 6, where mutual inductance M is determined by the actual road condition and carrying capacity in the movement,

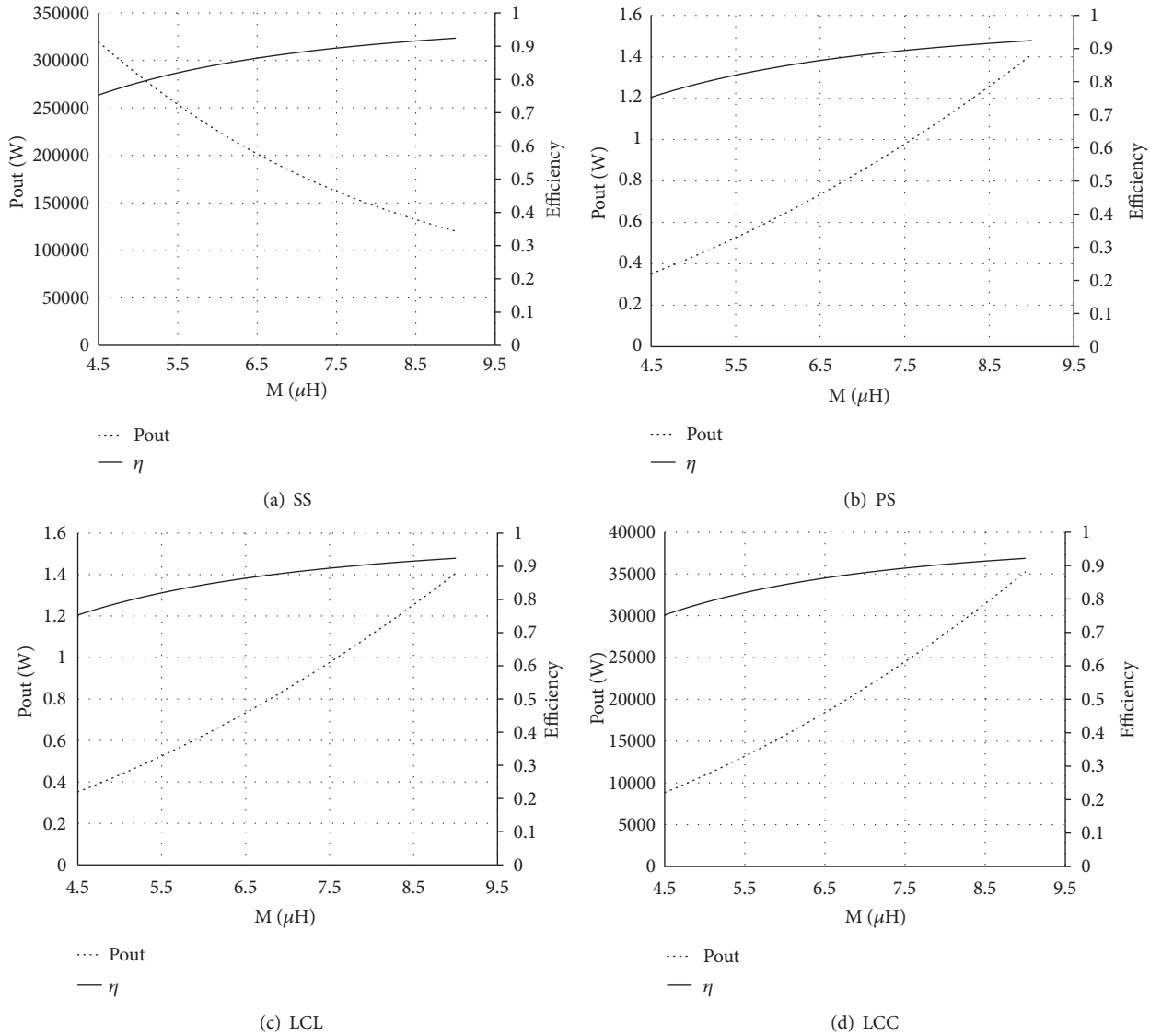

Figure 5: Output power and efficiency vary with mutual inductance.

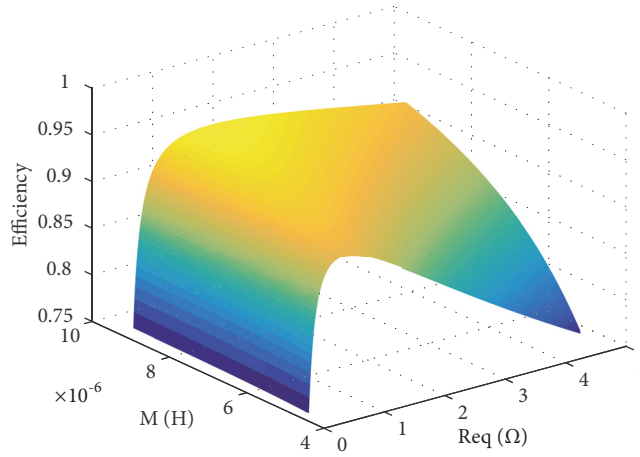

Figure 6: Efficiency varies with mutual inductance and load.

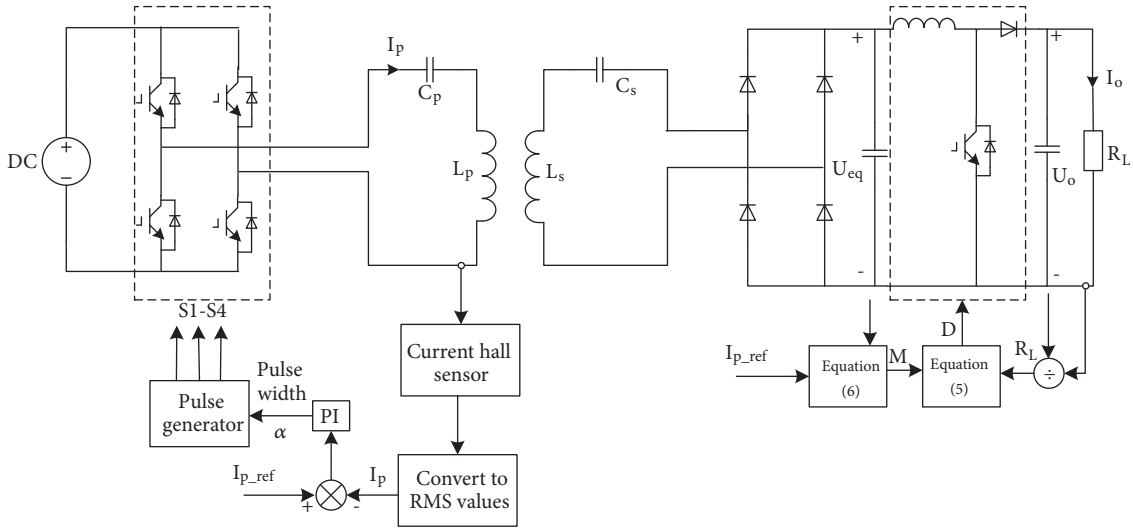

Figure 7: Decoupling control block diagram.

and it is an uncontrollable quantity. As can be seen from the image, for each mutual inductance, there is an equivalent resistance value to optimize the efficiency.

Taking the derivative of the efficiency with respect to the load ($d\eta/dR_{eq} = 0$), the load resistance expression when the system reaches the optimal efficiency can be obtained as

$$R_{eq_{opt}} = \omega M \sqrt{\frac{R_s}{R_p}} \tag{2}$$

According to the topology shown in Figure 1, the relationship between the system equivalent load and the actual load R_L of the system is as follows:

$$R_{eq} = \frac{8}{\pi^2} (1 - D)^2 R_L \tag{3}$$

Combining (2) with (3), the duty cycle of boost DCDC should meet the following formula in order to maintain high-efficiency output of the system:

$$\omega M \sqrt{\frac{R_s}{R_p}} = \frac{8}{\pi^2} (1 - D)^2 R_L \tag{4}$$

So duty cycle D is

$$D = 1 - \sqrt{\omega M \frac{\pi^2}{8R_L} \sqrt{\frac{R_s}{R_p}}} \tag{5}$$

Therefore, the system can track the load with the optimal efficiency through (5). However, since the mutual inductance value M in the equation is uncontrollable and unmeasurable, it needs to be calculated through measurable quantities. According to the secondary side induced voltage formula $U_s = j\omega MI_p$, the relationship between the output voltage U_{eq} of the secondary side rectifier and the current of the primary side conforms to the following relationship [12]:

$$U_{eq} = \frac{\sqrt{2}\pi}{4} j\omega M I_p \tag{6}$$

Therefore, if the duty cycle of boost DCDC remains in (5) relation with mutual inductance and load changes, the system can realize the optimal efficiency tracking strategy based on load matching.

4. Decoupling Control

In the application of dynamic wireless charging in urban rail transit, the primary and secondary side coils are in the process of relative movement, so it is relatively difficult to establish reliable real-time communication, and it is easy to be interfered by electromagnetic transmission process, resulting in large errors. And during dynamic power supply, in order to ensure the supply of load and battery energy storage, the inductive power transmission system should always work with the maximum rated transmission power that can be obtained [13, 14]. Based on this, the primary and secondary sides are decoupled from each other and independent control strategy block diagram is established, as shown in Figure 7.

The primary side adjusts the output voltage pulse width of the inverter through PI closed-loop to realize constant current control of the current of the primary side coil. The transmitting coil current I_p is collected by the current hall sensor and converted into the RMS value. The error value is obtained by subtracting I_{p_ref} from the set value of the RMS. The error value is transmitted to PI controller to obtain the control value pulse width α, and then the pulse width generator is used to control the output voltage pulse width of the inverter, so as to control the constant current of the primary side coil and realize the system to work with the maximum rated transmission power that can be obtained. At the same time, the rectification output voltage U_{eq} is detected by the secondary side. According to the formula (6) of the secondary side induced coupling voltage and the current setting value of the primary side, the mutual inductance M under the current running state of the vehicle can be

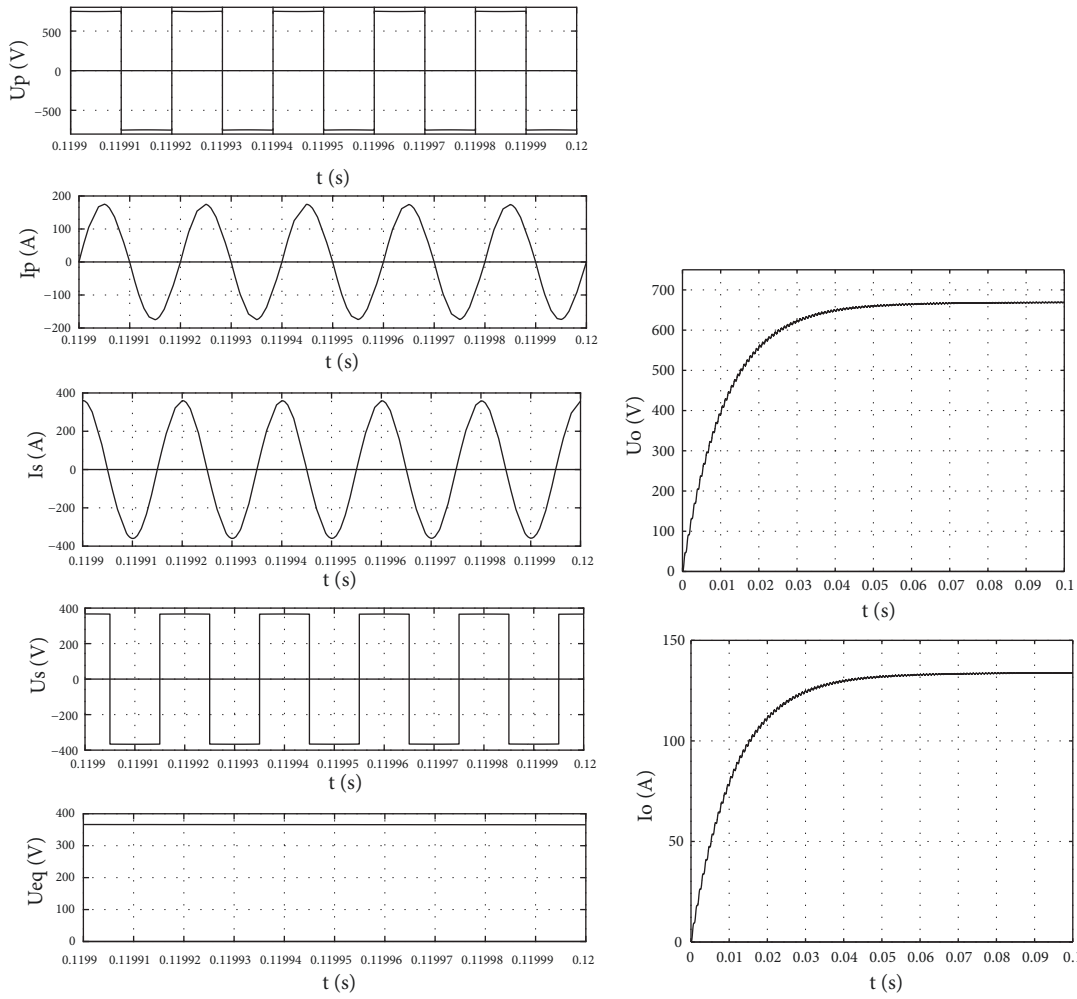

(a) Voltage and current of the primary and secondary sides

(b) Output voltage and current

Figure 8: Simulation waveform.

obtained. The current load value is calculated by detecting the output voltage and current of the output terminal. Based on the current mutual inductance M and resistance RL, the duty cycle D with the optimal efficiency matching is deduced through (5) to control the duty cycle of the boost DCDC converter, so as to realize the closed-loop control of the secondary side, realize the output of the system's maximum efficiency, cancel the information communication of the original auxiliary side, and realize decoupling control.

5. The Simulation Verification

In order to verify the original side decoupling control strategy based on optimal efficiency load tracking proposed in this paper, the MATLAB/Simulink simulation tool was used to build the system model. The system parameters were based on the high-power inductive power transmission system applied to urban rail transit. The simulation parameters were set as shown in Table 3. The simulation waveform is shown in Figure 8.

Under this control strategy, the equivalent load of the system keeps track of mutual inductance changes, so that the system always maintains high-efficiency output, and the primary and secondary sides are decoupled. The theoretical calculation value and simulation value of system output power and transmission efficiency changing with mutual inductance are compared as shown in Figures 9 and 10.

As can be seen from the image, the simulation results are roughly consistent with the theoretical calculation values. The output power varies linearly with the mutual inductance value. The higher mutual inductance value corresponds to the higher output power. In addition, the transfer efficiency of the coupling mechanism can be maintained at more than 90% within the range of mutual inductance that can be achieved by the coupling mechanism, which verifies the effectiveness of the control strategy.

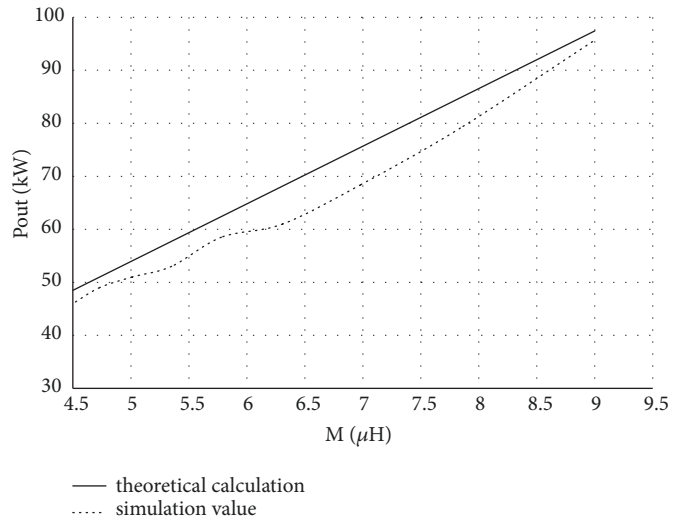

Figure 9: The output power of theoretical calculation and simulation value.

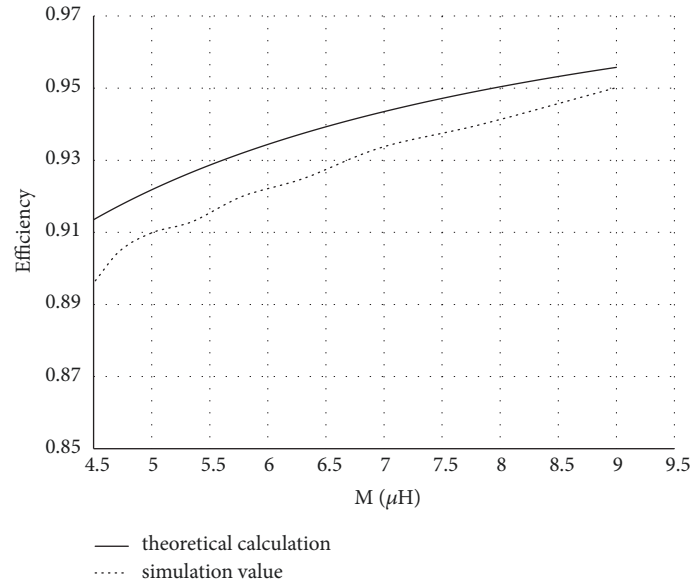

Figure 10: The transmission efficiency of theoretical calculation and simulation value.

Table 3: System simulation parameters.

Parameters	Value
DC voltage U_{DC}/V	750
Maximum power P_{max}/kW	100
Frequency f/kHz	50
Primary coil self-induction $L_p/\mu H$	160,8
Secondary coil self-induction $L_s/\mu H$	91
Primary coil self-resistance $R_p/m\Omega$	13,10
Secondary coil self-resistance $R_s/m\Omega$	3,12
Primary compensation capacitance C_p/nF	63,07
Secondary compensation capacitance C_s/nF	111,45
Load resistance R_L/Ω	5
Mutual inductance $M/\mu H$	4,5-9,0

6. Conclusion

The inductive power transmission system is applied to the dynamic situation of urban rail transit, which puts forward strict requirements on its energy output capacity and stability. Moreover, it is relatively difficult to establish reliable real-time communication due to the short time interaction. Based on this, this paper proposes the decoupling control strategy of the primary and secondary sides based on the optimal efficiency load tracking for the high-power dynamic inductive power system, so that the primary and secondary side communication can be cancelled in the inductive power transmission system and independent decoupling control can be realized. Simulation results show that the control method proposed in this paper can realize decoupling control of the system, the control of output power of the primary side through a closed loop, and the load tracking of the optimal efficiency of the secondary side. The results show that the control method is feasible and effective and has high engineering application value.

Data Availability

The Control Ideas of reference ([2–15]) data used to support the findings of this study have been deposited in the [DOI] repository. The Control Ideas of reference ([1]) data used to support the findings of this study were supplied by [CNKI] under license and so cannot be made freely available. Requests for access to these data should be made to CNKI [WWW.CNKI.COM.CN].

Conflicts of Interest

The authors declare that they have no conflicts of interest.

Acknowledgments

The project presented in this article is supported by the National Key Research and Development Program (2017YFB1201003-014).

References

[1] L. Pugi, A. Reatti, and F. Corti, "Application of wireless power transfer to railway parking functionality: preliminary design considerations with series-series and LCC topologies," *Journal of Advanced Transportation*, vol. 2018, Article ID 8103140, 14 pages, 2018.

[2] T. Yong, *Research on key issues of sectional track-based wireless power supply technology for electric vehicles*, Doctoal thesis of Chongqing University, 2012.

[3] Z. Jinbo, C. Tao, D. Shanxu et al., "A T-type high misalignment tolerant compensated topology for sectional track-based dynamic wireless power transmission system," *Transactions of China Electrotechnical Society*, vol. 32, no. 18, pp. 36–43, 2017.

[4] C. Wang, O. H. Stielau, and G. A. Covic, "Design considerations for a contactless electric vehicle battery charger," *IEEE Transactions on Industrial Electronics*, vol. 52, no. 5, pp. 1308–1314, 2005.

[5] G. L. Fischer and H. Doht, "An inverter system for inductive tube welding utilizing resonance transformation," in *Proceedings of 1994 IEEE Industry Applications Society Annual Meeting*, pp. 833–840, IEEE, 1994, https://doi.org/10.1109/IAS.1994.

[6] C.-S. Wang, G. A. Covic, and O. H. Stielau, "Investigating an LCL load resonant inverter for inductive power transfer applications," *IEEE Transactions on Power Electronics*, vol. 19, no. 4, pp. 995–1002, 2004.

[7] Z. Pantic, S. Bai, and S. Lukic, "ZCS-compensated resonant inverter for inductive-power-transfer application," *IEEE Transactions on Industrial Electronics*, vol. 58, no. 8, Article ID 2081954, pp. 3500–3510, 2011.

[8] F. Manyi, S. Liming, Y. Zhenggang et al., "Research on control strategy of segmented power supply for mobile inductive power transfer system," *Transaction of China Electrotechnical Society*, vol. 33, no. 17, Article ID 171230, pp. 3998–4006, 2018.

[9] A. Ayachit, F. Corti, A. Reatti, and M. K. Kazimierczuk, "Zero-voltage switching operation of transformer class-E inverter at any coupling coefficient," *IEEE Transactions on Industrial Electronics*, vol. 66, no. 3, pp. 1809–1819, 2019.

[10] Y.-G. Su, S. Zhang, C. Hu, C.-S. Tang, and W. Zhou, "An embeddable transmitter coil applied to electric vehicles powered by IPT system," *International Journal of Applied Electromagnetics and Mechanics*, vol. 50, no. 4, pp. 627–636, 2016.

[11] C. Hua, S. Liming, and L. Yaohua, "Output power adjustment in inductively coupled power transfer system," *Transaction of China Electrotechnical Society*, vol. 29, no. 1, pp. 215–220, 2014.

[12] L. W. Zhang, Y. Yang, M. H. Sun et al., "Energy management strategy based on dynamic programming for dual source trolleybus," *Tehnicki vjesnik / Technical Gazette*, vol. 24, no. 5, pp. 1439–1447, 2017.

[13] T. Batra, E. Schaltz, and S. Ahn, "Effect of ferrite addition above the base ferrite on the coupling factor of wireless power transfer for vehicle applications," *Journal of Applied Physics*, vol. 117, no. 17, Article ID 4919039, p. 4, 2015.

[14] M. Budhia, J. T. Boys, G. A. Covic, and C.-Y. Huang, "Development of a single-sided flux magnetic coupler for electric vehicle IPT charging systems," *IEEE Transactions on Industrial Electronics*, vol. 60, no. 1, pp. 318–328, 2013.

[15] Y. Qingxin, C. Haiyan, X. Guizhi et al., "Research progress in contactless power transmission technology," *Transaction of China Electrotechnical Society*, vol. 25, no. 7, pp. 6–13, 2010 (Polish).